J Mater Sci (2017) 52:2889–2894

Evidence of mixed valence Cr^{+3}/Cr^{+4} in $Y_{1-x}Ca_xCrO_3$ polycrystalline ceramics by X-ray photoelectron spectroscopy

R. Escamilla[1,*], L. Huerta[1], M. Romero[2], E. Verdin[3], and A. Durán[4]

[1] *Instituto de Investigaciones en Materiales, Universidad Nacional Autónoma de México, Apartado Postal 70-360, México, D.F. 04510, Mexico*

[2] *Facultad de Ciencias, Universidad Nacional Autónoma de México, Apartado Postal 70-399, 04510 México, D.F., Mexico*

[3] *Departamento de Física, Universidad de Sonora, Apartado Postal 1626, CP 83000 Hermosillo, SON, Mexico*

[4] *Centro de Nanociencias y Nanotecnología, Universidad Nacional Autónoma de México, Km. 107 Carretera Tijuana-Ensenada, Apartado Postal 14, C.P. 22800 Ensenada, BC, Mexico*

Received: 15 August 2016
Accepted: 8 November 2016
Published online: 16 November 2016

© Springer Science+Business Media New York 2016

ABSTRACT

$Y_{1-x}Ca_xCrO_3$ polycrystalline ceramics with $0.000 \leq x \leq 0.100$ compositions were studied by X-ray diffraction (XRD) and X-ray photoelectron spectroscopy (XPS). The results revealed that the ⟨Cr–O⟩ average bond length decreases with increasing Ca content. This fact infers that the charge compensation is through the change from Cr^{+3} to Cr^{+4} instead of oxygen vacancies. To confirm this supposition, the high-resolution XPS study revealed that as the Ca is introduced in the $YCrO_3$ matrix, the Cr $2p_{3/2}$ core-level is well fitted at 576.22 and 577.57 eV belonging at Cr^{+3} and Cr^{+4} core-level, respectively. Furthermore, we found an increase of the valence band XPS spectra at the Fermi energy as the Ca replaces the Y site. This fact suggests an increase of the Cr 3*d*-state at the Fermi energy, which is confirmed by the XPS valence band spectra and the electrical conductivity measurements.

Introduction

There has been considerable interest in the orthochromites in the past years as a result of biferroics properties found in some members of this family [1–3]. In these materials, the coupling between the magnetization and the polarization allows an additional degree of freedom in the design of a novel device for technological applications, such as magneto-optic, spintronic, and data storage device [4–6]. $YCrO_3$, for example, has the following crystalline and physical properties: (i) crystallize in perovskite-type compound, which has an orthorhombic $GdFeO_3$-type crystal structure at room temperature with a space group *Pbnm*; (ii) the dominant spin–spin interaction is through the Cr^{+3} ($3d^3$: $t_{2g}^3 e_g^0$) states, which is antiferromagnetically coupled with nearest

Address correspondence to E-mail: rauleg@unam.mx

DOI 10.1007/s10853-016-0582-4

neighbors of the Cr^{+3} moments at about T_N = 142 K [3, 7]; (iii) a slight displacement of Cr ions appears to be responsible for the weak ferroelectricity at room temperature, although its ferroelectric origin is still under discussion [1, 3, 8]. On the other hand, several studies are available in the literature [9–13] on its magnetic and transport properties after doping with trivalent and divalent ions at the Y or La site in the compounds (Y, La)CrO_3. Usually, the total solubility is obtained when the rare earth replaces the no magnetic La or Y ions. Below of T_N, the partial $La_{1-x}R'_xCrO_3$ R=Pr, Ce solubility have shown exotic magnetic ground state [9, 14]. On the other hand, the divalent ions (Ca, Sr) doped in the (Y, La)CrO_3 structures have shown a limited of solubility in the host matrix. Furthermore, the antiferromagnetic transition is suppressed with the substitution of these divalent ions, whereas the electrical properties showed the thermally activated conductivity process [11, 12, 15, 16]. The number of charge carriers increases as Ca or Sr ions are gradually introduced in the $YCrO_3$ matrix. The mobility is exponentially temperature dependent, and in many cases, the transport is via the hopping motion of spatially localized charge carriers. For example, the charge carriers' mobility is believed to arise from lattice distortion localization, i.e., small polarons formation or by stoichiometric defects varying the oxygen content (cation vacancies) in $Y_{1-x}Ca_xCrO_3$ [17]. We have recently argued that the charge compensation takes place via the Cr^{+3} to Cr^{+4} ions instead of charge compensation by the creation of oxygen vacancies as Ca is replaced by Y ion [18]. This affirmation was established indirectly through continuous decreasing of average ⟨Cr–O⟩ bond length. However, it is essential to state the true nature of the Cr environment as Ca is substituted by Y site. To overcome this issue, we resort to X-ray photoelectron spectroscopy technique which is widely used in the analysis of the oxidation states and the valence band of the involved chemical species in the ceramic compound. Although the electronic properties of $YCrO_3$ have been well studied [19, 20], details of the effect of substitution of Ca in the Y sites on the electronic structure have not yet been carried out. For this reason, we have performed the X-ray photoelectron spectroscopy in the $Y_{1-x}Ca_xCrO_3$ with $0.000 \leq x \leq 0.100$. The purpose is elucidated the chromium chemical environment as well as the effect of Ca on the Cr 3*d* state at the energy Fermi level through the valence band spectrum.

Experimental details

Polycrystalline samples of $Y_{1-x}Ca_xCrO_3$ with x = 0.000, 0.025, 0.050, and 0.100 compositions were synthesized by combustion method. The synthesis details can be found elsewhere [20]. Phase identification of the samples was performed with a Siemens D-5000 diffractometer with Cu Kα radiation and Ni filter. Measurements were performed in steps of 0.02° for 14 s in the 2θ range of 5° – 120° at room temperature. The crystallographic phases were identified with the JCPDS database. Structural parameters were refined by the Rietveld method using the QUANTO program with multi-phase capability [21]. The electronic structure and the chemical analysis were carried out by X-Ray photoelectron spectroscopy (XPS) using a UHV system of VG Microtech ESCA2000 Multilab, with an Al K X-ray source (hν = 1486.6 eV) and CLAM4 MCD analyzer. The surface of polycrystalline samples was etched for 10 min with 4.5 kV Ar^+ at 0.33 μA mm^{-2}. The XPS spectra were obtained at 55^o to the normal surface in the constant pass energy mode (CAE), E_0 = 50 and 20 eV for surface and high-resolution narrow scan, respectively. The peak positions were referenced to the C 1*s* core-level of the hydrocarbon groups localized at 284.50 eV. The XPS spectra were fitted using the SDP v 4.1 program [22]. The quality of fit is determined by a parameter called chi-square (χ^2), and for good fits, this value is <2.0. The uncertainty estimated in XPS deconvolution analyzes is 5% (i.e., ± 0.05 eV). The electrical conductivity was carried out using an LCR (HP 4284 A) bridge from 1 to 50 kHz.

Results and discussion

Figure 1 shows the powder X-ray diffraction patterns of the polycrystalline samples $Y_{1-x}Ca_xCrO_3$ with x = 0.000, 0.025, 0.050, and 0.100 at room temperature. In all samples, the patterns show a single phase that corresponds to the distorted perovskite structure with orthorhombic symmetry (ICSD N° 34-0365). The X-ray diffraction patterns of the samples were

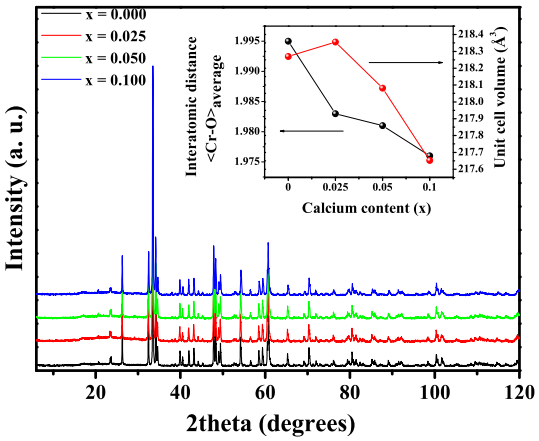

Figure 1 X-ray diffraction patterns for the polycrystalline samples $Y_{1-x}Ca_xCrO_3$ with x = 0.000, 0.025, 0.050, and 0.100. The *inset* shows the unit cell volume and the ⟨Cr–O⟩ average as a function of calcium content.

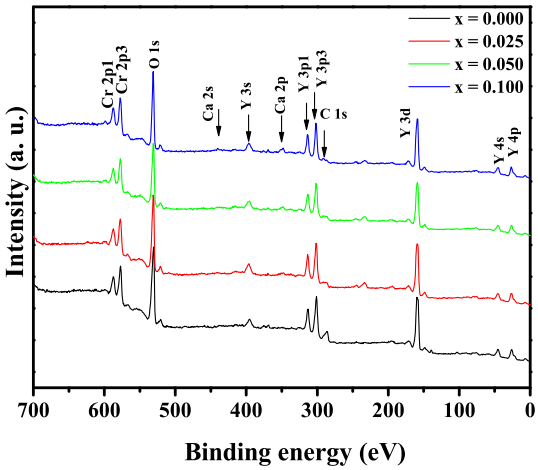

Figure 2 XPS survey spectra after Ar^+ etching for the polycrystalline samples $Y_{1-x}Ca_xCrO_3$.

Rietveld-fitted using a space group *Pbnm* (N° 62), taken into account the possibility that Ca occupies Y sites. The structural parameters obtained were reported in the reference [18]. In the inset of Fig. 1, a decrease in the unit cell volume as a function of Ca content is observed, which is contrary to the expected result, since the effective ionic radius of Y^{+3} (1.019 Å) is lower than that of Ca^{+2} (1.126 Å) ion with eight coordination number [23]. This unexpected result was attributed to the charge increased from Cr^{+3} (0.615 Å) to Cr^{+4} (0.550 Å) in the octahedral environment [24]. The change of valence state was experimentally deduced by decreasing of the volume and particularly the ⟨Cr–O⟩ average bond length as it is clearly shown in the inset of Fig. 1. This indirect result needs to be elucidated; for this purpose, we have studied the core-level by X-ray photoelectron spectroscopy (XPS) to determine the valence state of the ions in the doped structure.

Figure 2 shows the XPS survey spectra from 0 to 700 eV after Ar^+ etching for the polycrystalline samples $Y_{1-x}Ca_xCrO_3$, before performing high-resolution scan on the Cr 2*p* core-level (CL). The elements of Y, Ca, Cr, and O were detected in the doped compound survey spectra. Additionally, the C 1s signal is found presumably due to external contamination. The high-resolution spectra for the Y $3d_{5/2}$, Ca $2p_{3/2}$, Cr $2p_{3/2}$, and O 1*s* were measured (not shown) and the core-level binding energies (CLBE) values are summarized in Table 1.

For x = 0.000, the Y $3d_{5/2}$ and Cr $2p_{3/2}$ CLBE are localized at 157.01 and 576.22 eV, respectively. The

Table 1 Lattice parameters and unit cell volume for the samples $Y_{1-x}Ca_xCrO_3$ Ref. [18]

Calcium content (x)	a(Å)	b(Å)	c(Å)	V(Å^3)
0.000	5.2437(3)	5.5235(3)	7.5360(2)	218.270
0.025	5.2467(3)	5.5221(2)	7.5366(3)	218.356
0.050	5.2445(1)	5.5196(1)	7.5337(2)	218.082
0.100	5.2477(2)	5.5090(2)	7.5287(3)	217.652

value of Y $3d_{5/2}$ CLBE is higher than that the associated to Y_2O_3 (NIST XPS database [25]: Y $3d_{5/2}$: 156.4–156.9 eV, average 156.65 eV), whereas the corresponding Cr $2p_{3/2}$ CLBE is similar to the Cr_2O_3 (NIST XPS database: Cr $2p_{3/2}$: 576.0–577.1 eV, average 576.55 eV). These values show that the ions are in states Y^{3+} and Cr^{3+}. On the other hand, the O 1s CLBE is localized at 529.51 eV, and similar results are observed in the reference [26]. For x = 0.025, the Ca $2p_{3/2}$ CLBE is localized at 346.94 eV, indicating that the ions are in valence Ca^{2+}.

Figure 3a shows the comparison of high-resolution XPS spectra of Cr 2*p* CL fitted for x = 0.000 and 0.100. From x = 0.025 to 0.100, the precise shape of Cr $2p_{3/2}$ CL is fitted assuming the contribution of two components belonging to two different chemical states of the Cr. The Cr $2p_{3/2}$ CLBE was localized at 576.22 eV (FWHM 3.45 eV) and 577.57 eV (FWHM 3.42 eV) that might be attributed to Cr^{3+} and Cr^{+4}, respectively (see Fig. 3(b)). The value of χ^2 obtained for Cr 2*p* XPS spectra fitted was <0.9.

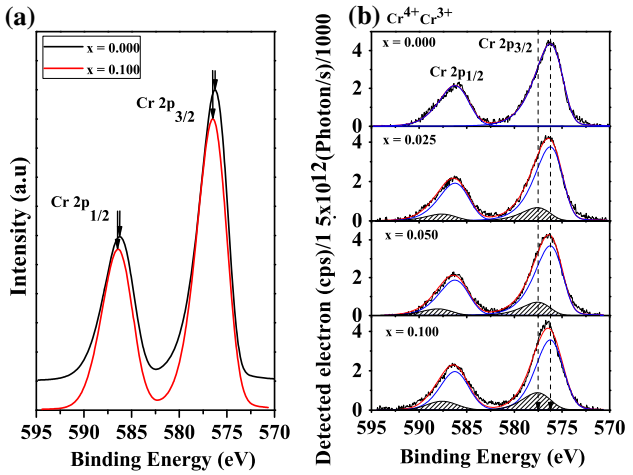

Figure 3 **a** Comparison of XPS spectra of Cr 2p fitted for x = 0.000 and 0.100. *Arrows* indicate the peak position. **b** Deconvolution of high-resolution XPS spectra of the Cr 2*p* core-levels of all samples. The *shadowed area* in the Cr 2*p* panel corresponds to Cr^{+4}.

These results are consistent with values obtained for the chromium trioxide (Cr_2O_3) and chromium dioxide (CrO_2) thin films deposited by RF sputtering [27, 28]. On the other hand, it is observed that the intensity of the contribution Cr^{+4} respect to Cr^{+3} is increased as Ca content increases. Thus, the XPS analysis shows that the Ca content induces a mixed valence in the Cr ions, which explain the decreases of the ⟨Cr–O⟩ average bond length obtained by the Rietveld refinement. To obtain deeper insight into the relationship of the mixed valence state with the electronic structure, we analyze the XPS valence band spectra (Table 2).

Figure 4 shows the XPS valence band spectra for all samples. For a better interpretation of the spectroscopic data, the XPS valence band spectra are compared with the theoretical electronic density of states (DOS) of $YCrO_3$ determined from the band structure calculations [20]. The contributions of the O 2*p* states

Table 2 Core-level binding energies (CLBE) the polycrystalline samples $Y_{1-x}Ca_xCrO_3$. All values are in eV

Calcium content (x)	Y $3d_{5/2}$	Ca $2p_{3/2}$	Cr $2p_{3/2}$		O 1*s*
		Cr^{3+}	Cr^{+4}		
0.000	157.01	–	576.22	–	529.51
0.025	157.69	346.94	576.22	577.57	530.04
0.050	157.69	347.21	576.22	577.57	530.04
0.100	157.87	347.26	576.22	577.57	530.33

to DOS are localized between −1.9 and −6.4 eV, whereas the DOS between −3.1 and −6.0 eV is due to the Y 3*d* states. Finally, near the Fermi level, the calculated DOS is formed mainly by Cr 3*d* states. As expected, a good correspondence between XPS valence band and DOS is obtained. It is observed that the DOS at the Fermi level $N(E_F)$ has slight increase as a consequence of increase calcium content. This fact suggests that the charge population of the Cr 3*d* state is increased with the induced mixed valence (Cr^{+3}, Cr^{+4}) with Ca doping. This result shows a good correspondence with the transport properties, particularly with the conductivity measurements.

Figure 5 shows the conductivity values for Ca content at 300 and 400 K. The conductivity was calculated considering the capacitance, and the dielectric loss as was obtained in Ref. [15]. The AC conductivity is increased with the Ca content and temperature. The increase of the conductivity at room temperature (300 K) with increasing Ca content is due to the change Cr^{+3}/Cr^{+4}, which is also evidenced by the increasing of the XPS valence band at $N(E_F)$ as seen in the inset of Fig. 4. The primary parameter that affects the electronic structure is the octahedral-site distortion which is deduced from the decrease of the average ⟨Cr–O⟩ bond length as calcium ions substitute yttrium sites. J. S. Zhou et al. [29] have shown that the CrO_6 octahedral in the orthorhombic perovskite is not rigid and the octahedral-site distortion tunes the electronic properties. In this case, the change from Cr^{+3} to Cr^{+4} observed by XPS explains

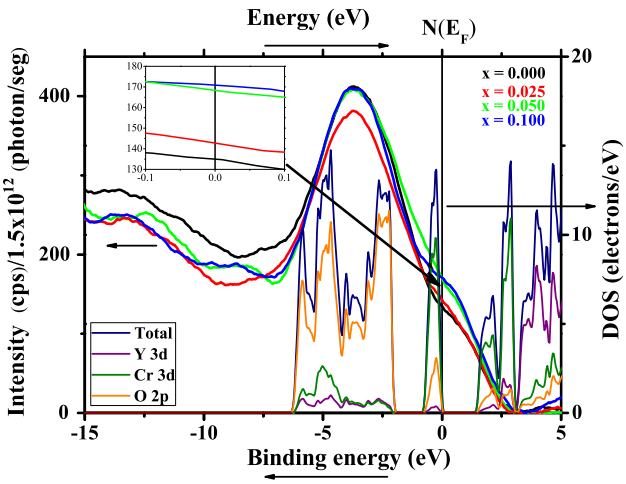

Figure 4 Comparisons of XPS Valence band and electronic density of states for $Y_{1-x}Ca_xCrO_3$. The scale on the *right side* corresponds to DOS and the *left* to XPS Valence band. *Inset* shows the zoom from −0.1 to 0.1 eV in the Valence band.

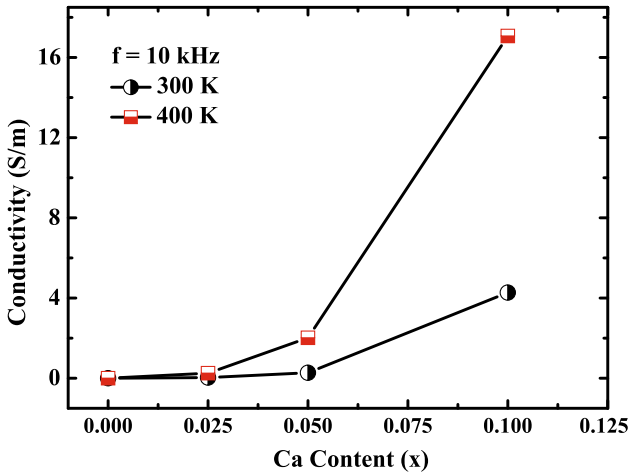

Figure 5 Calcium content (x) dependence of the electrical conductivity at 300 and 400 K. The electrical conductivity was calculated using the capacitance (Cp) and the dielectric loss (tan δ) at each frequency (ωi) according to the formula: $\sigma_{\omega i}(T) = \frac{l}{s}\omega_i Cp_{\omega i}(T)\tan\delta_{\omega i}$ where 'l' is the thickness and 's' the area, respectively.

the decrease of the cell volume and particularly the decreasing of average ⟨Cr–O⟩ bond length which in turn increases slightly the XPS valence band at Fermi level via the octahedral-site distortion. On the other hand, the AC electrical conductivity is thermally activated above of 300 K, and the activation energy is consistent with conduction by small polarons [15]. These quasiparticles increase with Ca content, and they are activated with temperature resulting in an increasing in the electrical conductivity. W. J. Webber [12] showed that the small polarons as charge carrier are the principal mechanism participating in the temperature dependence of the electrical conductivity in $Y_{1-x}Ca_xCrO_3$ and $La_{1-x}Ca_xCrO_3$ [17]. This fact occurs if the charge carriers are self-trapped in the distort surrounding lattice, which in this case are localized in the Cr^{+4} environment. Thus, the XPS study indicated that the charge compensation of the Y^{+3} by Ca^{+2} occurs through the Cr mixed valence instead of oxygen vacancies.

Conclusions

In this paper, polycrystalline samples of $Y_{1-x}Ca_xCrO_3$ with $x = 0.000$, 0.025, 0.050, and 0.100 were studied by X-ray diffraction (XRD) and X-ray photoelectron spectroscopy (XPS). High-resolution XPS spectra of the Cr $2p_{3/2}$ CL show experimental evidence of mixed valence states of Cr^{+3}/Cr^{+4}. Analysis of the valence band using XPS reveals that the calcium doping induces a systematic increase in the DOS at the Fermi level. Accordingly, the electrical conductivity increases because of the increase of the self-trapped charge as small polarons in the Cr^{+4} environment.

Acknowledgements

The authors thank the projects DGAPA-UNAM IN-103016 and IN-106116/27. They also thank F. Silvar, Adriana Tejeda-Cruz, M.M.S. Alberto Lopez-Vivas, A. Pompa, and C. Gonzalez for providing technical help. Calculations were performed using resources from the Supercomputing Center DGTIC-UNAM.

References

[1] Sahu JR, Serrao CR, Ray N, Waghmare UV, Rao CNR (2007) Rare earth chromites: a new family of multiferroics. J Mater Chem 17:42–44

[2] Rajeswaran B, Khomskii DI, Zvezdin AK, Rao CNR, Sundaresan A (2012) Field-induced polar order at the Nel temperature of chromium in rare-earth orthochromites: interplay of rare-earth and Cr magnetism. Phys Rev B 86:214409

[3] Serrao CR, Kundu AK, Krupanidhi SB, Waghmare UV, Rao CNR (2005) Biferroic $YCrO_3$. Phys Rev B 72:220101(R)

[4] Ramesh R (2010) Ferroelectrics: a new spin on spintronics. Nat Mater 9:380–381

[5] Ramesh R, Spaldin NA (2007) Multiferroics: progress and prospects in thin films. Nat Mater 6:21–29

[6] Bibes ABM (2008) Multiferroics: towards a magnetoelectric memory. Nat Mater 7:425–426

[7] Yamaguchi T, Tsushima K (1973) Magnetic symmetry of rare-earth orthochromites and orthoferrites. Phys Rev B 8:5187–5198

[8] Ramesha K, Llobet A, Proffen T, Serrao CR, Rao CNR (2007) Observation of local non-centrosymmetry in weakly biferroic $YCrO_3$. J Phys 19:102202

[9] Yoshii K, Nakamura A, Ishii Y, Morii Y (2001) Magnetic properties of $La_{1-x}Pr_xCrO_3$. J Solid State Chem 162:84–89

[10] Daniels LM, Weber MC, Lees MR, Guennou M, Kashtiban RJ, Sloan J, Kreisel J, Walton RI (2013) Structures and magnetism of the rare-earth orthochromite perovskite solid solution $La_xSm_{1-x}CrO_3$. Inorg Chem 52:12161–12169

[11] Neumeier JJ, Terashita H (2004) Magnetic, thermal, and electrical properties of $La_xCa_{1-x}CrO_3$ ($0 \le x \le 0.5$). Phys Rev B 70:214435

[12] Weber WJ, Griffin CW, Bates JL (1987) Effects of cation substitution on electrical and thermal transport properties of $YCrO_3$ and $LaCrO_3$. J Am Ceram Soc 70:265–270

[13] Subba Rao GV, Wanklyn BM, Rao CNRJ (1971) Electrical transport in rare earth ortho-chromites, -manganites and -ferrites. Phys Chem Solids 32:345–358

[14] Shukla R, Manjanna J, Bera AK, Yusuf SM, Tyagi AK (2009) $La_{1-x}Ce_xCrO_3$ ($0.0 \leq x \leq 1.0$): a new series of solid solutions with tunable magnetic and optical properties. Inorg Chem 48:11691–11696

[15] Durán A, Arévalo-López AM, Castillo-Martínez E, García-Guaderrama M, Moran E, Cruz MP, Fernández MP, Alario-Franco MA (2010) Magneto-thermal and dielectric properties of biferroic $YCrO_3$ prepared by combustion synthesis. J Solid State Chem 183:1863–1871

[16] Carini GF II, Anderson HU, Sparlin DM, Nasrallah MM (1991) Electrical conductivity, seebeck coefficient and defect chemistry of Ca-doped $YCrO_3$. Solid State Ion 49:233–243

[17] Webb JB, Sayer M, Mansingh A (1977) Polaronic conduction in lanthanum strontium chromite. Can J Phys 55:1725–1731

[18] Durán A, Verdin E, Escamilla R, Morales F, Escudero R (2012) Mechanism of small-polaron formation in the biferroic $YCrO_3$ doped with calcium. Mater Chem Phys 133:1011–1017

[19] Ray N, Waghmare UV (2008) Coupling between magnetic ordering and structural instabilities in perovskite biferroics: a first-principles study. Phys Rev B 77:134112

[20] Nair VG, Ganeshraj C, Santhosh PN, Subramanian V (2013) AIP Conf Proc 1512:846–847

[21] Altomare A, Burla MC, Giacovazzo C, Guagliardi A, Moliterni AGG, Polidori G, Rizzi R (2001) Quanto: a Rietveld program for quantitative phase analysis of polycrystalline mixtures. J Appl Crystallogr 34:392–397

[22] SDP v4.1 (32 bit) Copyright XPS International, LLC, Compiled 17 January (2004)

[23] Shannon RD (1976) Revised effective ionic radii and systematic studies of interatomic distances in halides and chalcogenides. Acta Crystallogr A 32:751–767

[24] Castillo-Martinez E, Durán A, Alario-Franco MA (2008) Structure, microstructure and magnetic properties of $Sr_{1-x}Ca_xCrO_3$ ($0 \leq x \leq 1$). J Solid State Chem 181:895–904

[25] NIST X-ray Photoelectron spectroscopy database, Version 4.1 (National Institute of Standards and Technology, Gaithersburg, 2012); http://srdata.nist.gov/xps/

[26] Zhang B, Zhao Q, Chang A, Li Y, Liu Y, Wu Y (2014) Electrical conductivity anomaly and X-ray photoelectron spectroscopy investigation of $YCr_{1-x}Mn_xO_3$ negative temperature coefficient ceramics. Appl Phys Lett 104:102109

[27] Cheng R, Xu B, Borca CN, Sokolov A, Yang CS, Yuan L, Liou SH, Doudin B, Dowbena PA (2001) Characterization of the native Cr_2O_3 oxide surface of CrO_2. Appl Phys Lett 79:3122–3124

[28] Bullen Heather A, Garrett Simon J (2001) CrO_2 by XPS: Comparison of CrO_2 Powder to CrO_2 Films on TiO_2(110) Single Crystal Surfaces. Surf Sci Spectra 8:225–233

[29] Zhou J.-S, Goodenough J. B. (2008) Intrinsic structural distortion in orthorhombic perovskite oxides. Phys Rev B 77:132104